XL CILAMCE
IBERO-LATIN AMERICAN CONGRESS ON COMPUTATIONAL METHODS IN ENGINEERING
NOVEMBER 11-14, 2019
Praiamar Natal Hotel & Convention
Natal, RN-BRAZIL

IMPROVED NUMERICAL SIMULATION OF 2D FRAME STRUCTURES USING A GENERALIZED MODAL ANALYSIS

Ney A. Dumont
dumont@puc-rio.br
Rodrigo N. Barros
rodrigonb.eng@gmail.com
Carlos A. Aguilar
carlosampe@hotmail.com.com
Department of Civil and Environmental Engineering
PUC-Rio – Pontifical Catholic University of Rio de Janeiro
22451-900 Rio de Janeiro, Brazil

Abstract. The hybrid finite element method, proposed by Pian on the basis of the Hellinger-Reissner potential, has proved itself a conceptual breakthrough among the discretization formulations. A proposition made by Przemieniecki – for the generalized free vibration analysis of truss and beam elements – was incorporated into the hybrid finite/boundary element method developed by the third author and extended to the analysis of time-dependent problems by making use of an advanced mode superposition procedure that adequately takes into account general initial conditions as well as general body actions. It is shown that such a consistent approach leads to frequency-dependent stiffness and mass matrices that enter a generalized modal analysis based on a nonlinear eigenvalue problem for complex-symmetric systems. This paper presents the basic features of the formulation as applied to plane frame structures and assesses some examples available in the technical literature to show that remarkable improvements may be achieved with the proposed formulation when compared to the classical structural dynamics. Although the formulation is generally valid for three-dimensional analysis, owing to space restrictions only two-dimensional plane frames and trusses are dealt with. The analytical frequency-domain expressions of beams with and without hinges on the extremities is displayed to make evident how axial and transversal modes interact and should be properly taken into account.

Keywords: Structural dynamics, Generalized modal analysis, Non linear eigenvalues

1 Introduction

An established technique to solve time-dependent problems other than directly dealing with the time variable is the formulation of a complete frequency-domain analysis via Laplace or Fourier transforms, with subsequent ad hoc expression of results by numerical inversion (Aguilar [1], Dumont and Aguilar [2], Dubner and Abate [3], Crump [4], De Hoog et al [5]). Although usually easy to implement, such a transform inversion is computationally intensive, if accurate results are to be obtained, and is not void of numerical instabilities. Moreover, the inclusion of non-homogeneous initial conditions and general body forces may become troublesome.

An alternative formulation is the modal analysis, which is mainly applied to structural dynamics and is based on the expansion theorem for continuous systems, according to which any sufficiently continuously differentiable function satisfying the boundary conditions of the problem can be represented by the absolutely and uniformly convergent series of the system's eigenfunctions.

The first author and collaborators have proposed to solve transient problems of potential and elasticity using an advanced mode superposition technique that applies to equilibrium-based finite element and boundary element models. The developments combine and extend Pian's hybrid finite element formulation [6] and Przemieniecki's suggestion of displacement-based, frequency-dependent elements [7], thus arriving at a hybrid finite/boundary element method for the general analysis of transient problems [8]. Starting from a frequency-domain formulation, it is shown that there is an underlying complex-symmetric (if viscous damping is included), non-linear eigenvalue problem related to the lambda-matrices of a free-vibration analysis, with an effective stiffness matrix expressed as the frequency power series of generalized stiffness, damping and mass matrices [9, 10]. The eigenvectors of this problem fulfill generalized orthogonality properties that enable the implementation of an advanced mode superposition technique. This leads to the solution in the time domain and the immediate expression of all results of interest. Since this is an equilibrium-based formulation, general domain actions (including body forces and moving loads) as well as boundary and initial conditions may be dealt with in a straightforward way.

The generalized modal analysis ends up having the same mathematical characteristics of the traditional one, except that the eigenvalue problem is solved more accurately and fewer degrees of freedom may become ultimately required in the practical solution of a given problem. The price to be paid is the evaluation of more coefficient matrices of the frequency power series.

The formulation is extremely advantageous in the analysis of framed structures, as it comes up that the classical proposition of one stiffness matrix and one mass matrix (and eventually one damping matrix) is just a – conceptually and numerically – unjustified series truncation. This is outlined in the paper, thus highlighting some improprieties in the classical text books. Owing to space restrictions only the frequency-dependent expressions for Euler-Bernoulli beams considering the four different cases of hinge end conditions are given explicitly.

Przemieniecki's displacement-based proposition of frequency-dependent truss and beam elements was the clear, however very initial, inspiration for the outlined general developments. Although a literature review is not intended herein, it should be mentioned that similar, however questionable and limited – both conceptually and in terms of applicability –, intents can be assigned to previous researchers, such as in the *dynamic element method* proposed by Voss [11] (see also Triebsch [12] and the questioning in the introductory part of Dumont [9]) and in the *component-mode method for trusses* proposed very early by Hurty [13], with similar developments by Craig and Bampton [14] and revisited by Weaver and Loh [15] and Weaver and Johnston [16].

2 Problem formulation

The following developments are already outlined in papers by the first author and co-workers [1, 2, 8 – 10, 17 – 22], although not as compact and objectively as here for the simplest case of Euler-Bernoulli beams (of which a truss element is a particularization). The conceptually paramount expressions of Section 2.2 are to the authors' best knowledge displayed for the first time in the

technical literature. It is worth observing that the following developments can be seamlessly obtained in the frame of a Laplace or Fourier transform [1]. The frequency term ω (physical meaning *rad/s*) to be introduced may just be seen as an in principle arbitrary separation constant, as given in the books on partial differential equations, with the complete time and space dependent problem eventually dealt with in terms of a modal analysis – in the present case a *generalized* or *advanced* modal analysis that must rely on the solution of a *generalized, non-linear eigenvalue problem* [10].

2.1 Basics for truss and beam elements

The general frequency-domain, small displacement solution $u(x)$ of a truss element of constant cross section *A*, elasticity modulus *E* and specific mass ρ is

$$u(x) = C_1 \frac{\sin k_N x}{k_N} + C_2 \cos k_N x\,, \tag{1}$$

where

$$k_N^2 = \frac{\rho}{E}\left(\omega^2 + 2i\zeta_N\omega\right) \tag{2}$$

and such that $\lim_{k_N \to 0} u(x) = C_1 x + C_2$. Viscous damping $2\zeta_N\rho$ (force by volume per unit velocity) in the axial direction is included just for the sake of completeness but will not be considered in the further developments.

The general frequency-domain, small transversal displacement solution $v(x)$ of a slender beam element in the Cartesian plane (x, y), for constant cross section *A*, elasticity modulus *E*, specific mass ρ, moment of inertia I_z and transversal viscous damping $2\zeta\rho$ is

$$v(x) = C_1 \frac{\cos kx + \cosh kx}{2} + C_2 \frac{\sin kx + \sinh kx}{2k} - C_3 \frac{\cos kx - \cosh kx}{k^2} - 3C_4 \frac{\sin kx - \sinh kx}{k^3}, \tag{3}$$

where

$$k^4 = \frac{\rho A}{EI_z}\left(\omega^2 + 2i\zeta\omega - \frac{\kappa}{\rho A}\right) \tag{4}$$

and such that $\lim_{k \to 0} v(x) = C_1 + C_2 x + C_3 x^2 + C_4 x^3$. Just for the sake of completeness, we include in the expression of k^4 the pressure κ exerted by an elastic (Winkler) foundation on the beam. A more general expression for the beam displacements should take into account the transversal shear effect (Timoshenko beam) as well as an eventual normal tensile force [1, 7]. However, we consider in the following developments only the effect of inertia forces for the transversal displacements of an Euler-Bernoulli beam, whose general solution is Eq. (3).

2.2 Stiffness matrices in the frequency domain

Equations (1) and (3) may be combined to compose a beam's stiffness matrix in the frequency domain, as referred to the natural system on the left of Fig. 1, which is oriented according to the beam's axial direction in the Cartesian plane. Four cases are given below depending on whether the beam is continuously linked or hinged to its adjacent part of the structure. The following array of matrices $\mathbf{K}_b$ has entries $i, j = 0, 1$, which are precisely the codes for continuity (0) or hinge (1) of a beam's left or right extremity. A more general case of the extremities connected to a spring with stiffening and viscous damping might be envisaged, but is not considered in this paper.

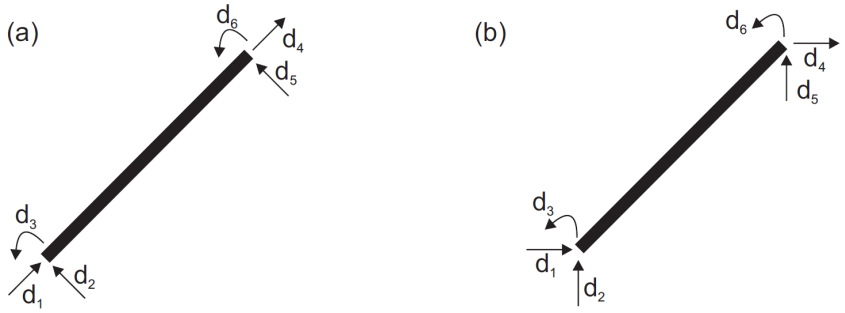

Figure 1. Locally- and globally-oriented coordinate systems of a bar element [25]

Case (0,0): Continuous beam at both extremities. The stiffness matrix of a bar continuously linked to adjacent bars at both extremities is expressed from Eq. (1) for the truss contribution in the coordinates 1 and 4 as well as from Eq. (3) for the beam contribution in the coordinates 2, 3, 5 and 6 as

$$\mathbf{K}_b(0,0) = EI_z \begin{bmatrix} \frac{Ac_Nk_N}{I_zs_N} & 0 & 0 & -\frac{Ak_N}{I_zs_N} & 0 & 0 \\ 0 & \frac{Sc+Cs}{1-Cc}k^3 & \frac{Ss}{1-Cc}k^2 & 0 & -\frac{S+s}{1-Cc}k^3 & \frac{C-c}{1-Cc}k^2 \\ 0 & \frac{Ss}{1-Cc}k^2 & \frac{Cs-Sc}{1-Cc}k & 0 & -\frac{C-c}{1-Cc}k^2 & \frac{S-s}{1-Cc}k \\ -\frac{Ak_N}{I_zs_N} & 0 & 0 & \frac{Ac_Nk_N}{I_zs_N} & 0 & 0 \\ 0 & -\frac{S+s}{1-Cc}k^3 & -\frac{C-c}{1-Cc}k^2 & 0 & \frac{Sc+Cs}{1-Cc}k^3 & \frac{-Ss}{1-Cc}k^2 \\ 0 & \frac{C-c}{1-Cc}k^2 & \frac{S-s}{1-Cc}k & 0 & \frac{-Ss}{1-Cc}k^2 & \frac{Cs-Sc}{1-Cc}k \end{bmatrix}, \quad (5)$$

where we introduce for the particular case of the local coordinate $x = \ell$, the bar's length, the simplifying notation from Eqs. (1) and (3):

$$s_N = \sin k_N\ell\,, \;\; c_N = \cos k_N\ell\,, \quad (6)$$

$$\mathrm{s} = \sin k\ell\,, \;\; \mathrm{c} = \cos k\ell\,, \;\; S = \sinh k\ell\,, \;\; \mathrm{C} = \cosh k\ell\,. \quad (7)$$

Case (1,0): Continuous beam on the right and hinged on the left. The stiffness matrix is obtained from the matrix of Eq. (5) by linear-algebra condensation of coordinate 3 given on the left of Fig. 1:

$$\mathbf{K}_b(1,0) = EI_z \begin{bmatrix} \frac{Ac_Nk_N}{I_zs_N} & 0 & 0 & -\frac{Ak_N}{I_zs_N} & 0 & 0 \\ 0 & \frac{Cc+1}{Cs-Sc}k^3 & 0 & 0 & -\frac{C+c}{Cs-Sc}k^3 & \frac{S+s}{Cs-Sc}k^2 \\ 0 & 0 & 0 & 0 & 0 & 0 \\ -\frac{Ak_N}{I_zs_N} & 0 & 0 & \frac{Ac_Nk_N}{I_zs_N} & 0 & 0 \\ 0 & -\frac{C+c}{Cs-Sc}k^3 & 0 & 0 & \frac{2Cc}{Cs-Sc}k^3 & -\frac{Cs+Sc}{Cs-Sc}k^2 \\ 0 & \frac{S+s}{Cs-Sc}k^2 & 0 & 0 & -\frac{Cs+Sc}{Cs-Sc}k^2 & \frac{2Ss}{Cs-Sc}k \end{bmatrix}. \quad (8)$$

Case (0,1): Continuous beam on the left and hinged on the right. The stiffness matrix is obtained from the matrix of Eq. (5) by linear-algebra condensation of coordinate 6 given on the left of Fig. 1:

$$\mathbf{K}_b(0,1) = EI_z \begin{bmatrix} \frac{Ac_N k_N}{I_z s_N} & 0 & 0 & -\frac{Ak_N}{I_z s_N} & 0 & 0 \\ 0 & \frac{2Cc}{Cs-Sc}k^3 & \frac{Cs+Sc}{Cs-Sc}k^2 & 0 & -\frac{C+c}{Cs-Sc}k^3 & 0 \\ 0 & \frac{Cs+Sc}{Cs-Sc}k^2 & \frac{2Ss}{Cs-Sc}k & 0 & -\frac{S+s}{Cs-Sc}k^2 & 0 \\ -\frac{Ak_N}{I_z s_N} & 0 & 0 & \frac{Ac_N k_N}{I_z s_N} & 0 & 0 \\ 0 & -\frac{C+c}{Cs-Sc}k^3 & -\frac{S+s}{Cs-Sc}k^2 & 0 & \frac{Cc+1}{Cs-Sc}k^3 & 0 \\ 0 & 0 & 0 & 0 & 0 & 0 \end{bmatrix}. \quad (9)$$

Case (1,1): Beam hinged at both extremities (truss). The stiffness matrix is obtained from the matrix of Eq. (5) by linear-algebra condensation of both coordinates 3 and 6 given on the left of Fig. 1:

$$\mathbf{K}_b(1,1) = EI_z \begin{bmatrix} \frac{Ac_N k_N}{I_z s_N} & 0 & 0 & -\frac{Ak_N}{I_z s_N} & 0 & 0 \\ 0 & \frac{Sc-Cs}{2Ss}k^3 & 0 & 0 & \frac{s-S}{2Ss}k^3 & 0 \\ 0 & 0 & 0 & 0 & 0 & 0 \\ -\frac{Ak_N}{I_z s_N} & 0 & 0 & \frac{Ac_N k_N}{I_z s_N} & 0 & 0 \\ 0 & \frac{s-S}{2Ss}k^3 & 0 & 0 & \frac{Sc-Cs}{2Ss}k^3 & 0 \\ 0 & 0 & 0 & 0 & 0 & 0 \end{bmatrix}. \quad (10)$$

Observe that not only the latter matrix for a truss element, but actually all matrices above accurately take into account frequency-dependent, longitudinal and transversal inertia effects: quite simpler than the approximate *component-mode method for trusses* proposed by Hurty [13, 14, 15]. It should be remarked that the longitudinal and transversal displacement shapes for a beam element – whether or not hinged – should also be accurately represented in the post-processing stage as the ones of the static analysis added by higher order polynomials that behave as bubble functions: this is obtained by just developing the displacements of Eqs. (1) and (3) as frequency power series and after expressing the constants in terms of the nodal degrees of freedom represented on the left of Fig. 1.

The rotation of the matrices above from the bar-oriented system on the left of Fig. 1 to the globally-oriented system on the right is a simple task. Assembling all elements' local stiffness matrices leads to a global, frequency-dependent effective stiffness matrix while conveniently eliminating coordinates to which no stiffening is attached (void global rotation-moment effects at hinges). This may be the seen as a procedure in the frame of Laplace or Fourier transforms [1]. (A similar development might be conceived for the time-domain analysis and consistently showing transversal cross effects for truss elements – which seems to be still explored technically.)

The following advanced modal analysis develops the matrices above as power series of the frequency ω (the λ – matrices referred to by Dumont [9] in a wider context), with as many terms as deemed adequate in a numerical simulation – and not just one term, as unconditionally shown in the text books on structural dynamics. Such power series developments can be easily carried out using symbolic mathematics and stored for sheer numerical coding, such as in Fortran. The symbolic developments in this paper have been done using Maple [26]. Some very simple illustrations of power series developments are shown by Dumont [9, 10], for instance.

3 Advanced modal analysis

Instead of formulating the problem for a prescribed frequency ω, as in a Laplace or Fourier transform, one expresses a structure's global effective stiffness matrix as a truncated power series of ω [1, 2, 8 – 10, 17 – 22]:

$$\mathbf{K} = \mathbf{K}_0 + \sum_{j=1}^{n} \omega^{2j} \mathbf{M}_j = \mathbf{K}_0 + \omega^2 \mathbf{M}_1 + \omega^4 \mathbf{M}_2 + \omega^6 \mathbf{M}_3 + \dots . \tag{11}$$

In this equation, $\mathbf{K}_0$ is explicitly given as the stiffness matrix of the static discrete-element formulation, and the remaining terms of the power series are renamed as generalized mass matrices, although they actually constitute a consistent blending of inertia and stiffness properties (Dumont [10] presents the complete complex-symmetric linear algebra structure of the problem including damping). In this way, the traditional dynamics equation becomes a more general differential equation of time,

$$\left(\mathbf{K}_0 - \sum_{j=1}^{n} (-1)^j \mathbf{M}_j \frac{\partial^{2j}}{\partial t^{2j}} \right) \Big(\mathbf{d}(t) - \mathbf{d}^b(t) \Big) = \mathbf{p}(t) - \mathbf{p}^b(t), \tag{12}$$

as here proposed for considering some particular solution $\Big(\mathbf{d}^b(t), \mathbf{p}^b(t) \Big)$, as for body forces, and for which the associate generalized, non-linear eigenvalue problem

$$\Big(\mathbf{K}(\omega) - \omega^2 \mathbf{M}(\omega) \Big) \mathbf{\Phi} = \mathbf{0} \tag{13}$$

must be solved. In this equation, the frequency-dependent stiffness and mass matrices are

$$\mathbf{K}(\omega) = \mathbf{K}_0 + \sum_{j=2}^{n} (j-1) \omega^{2j} \mathbf{M}_j = \mathbf{K}_0 + \omega^4 \mathbf{M}_2 + 2\omega^6 \mathbf{M}_3 + \dots , \tag{14}$$

$$\mathbf{M}(\omega) = \sum_{j=1}^{n} j \omega^{2j-2} \mathbf{M}_j = \mathbf{M}_1 + 2\omega^2 \mathbf{M}_2 + 3\omega^4 \mathbf{M}_3 + \dots , \tag{15}$$

as shown by Dumont [10]. The eigenpairs of this problem come out to satisfy the following generalized orthogonality and normalized conditions:

$$\sum_{j=1}^{n} \sum_{i=1}^{n} \mathbf{\Omega}^{2j-2i} \mathbf{\Phi}^{\mathrm{T}} \mathbf{M}_j \mathbf{\Phi}\, \mathbf{\Omega}^{2i-2} = \mathbf{I}, \tag{16}$$

$$\mathbf{\Phi}^{\mathrm{T}} \mathbf{K}_0 \mathbf{\Phi} + \sum_{j=1}^{n-1} \sum_{i=1}^{n-1} \mathbf{\Omega}^{2i} \mathbf{\Phi}^{\mathrm{T}} M_{j+1} \mathbf{\Phi}\, \mathbf{\Omega}^{2j} = \mathbf{\Omega}^2 . \tag{17}$$

Once the problem is solved, mode superposition of the nodal displacements is shown to be applicable [10],

$$\mathbf{d}(t) = \mathbf{\Phi}\, \boldsymbol{\eta}(t), \tag{18}$$

exactly as in the traditional structural dynamics, except that the eigenpairs are evaluated more accurately. The amplitudes $\boldsymbol{\eta}(t)$ are then obtained either analytically (Duhamel's integrals) or numerically, depending on the time expression of $\Big(\mathbf{p}(t) - \mathbf{p}^b(t) \Big)$, as an uncoupled set of second-order differential equations of time, as traditionally [10]:

$$\mathbf{\Omega}^2 \left(\boldsymbol{\eta} - \boldsymbol{\eta}^b \right) + \left(\ddot{\boldsymbol{\eta}} - \ddot{\boldsymbol{\eta}}^b \right) = \mathbf{\Phi}^{\mathrm{T}} \Big(\mathbf{p}(t) - \mathbf{p}^b(t) \Big). \tag{19}$$

3.1 Non-homogeneous initial conditions for damping-free problems

The more elaborated problem of considering non-homogeneous initial conditions for problems with viscous damping as well as some other conceptual issues are dealt with by Dumont [20, 24] and Dumont and Chaves [18]. Just for the sake of completeness we present an important remark concerning the adequate inclusion of non-homogeneous initial conditions as well as the evaluation of $\boldsymbol{\eta}^b$ from given nodal data $\mathbf{d}^b$ for the solution of Eq. (19). Let the subsets $\boldsymbol{\Phi}_{(el)}$ and $\boldsymbol{\Omega}_{(el)}$ of modes and frequencies be related to pure elastic deformation. The initial values at a time instant t_0 of displacement amplitudes $\boldsymbol{\eta}_{(el)}(t_0)$ and corresponding velocities $\dot{\boldsymbol{\eta}}_{(el)}(t_0)$ – to be considered in Eq. (19) – are obtained from initial nodal displacements $\mathbf{d}_{(el)}(t_0)$ and velocities $\dot{\mathbf{d}}_{(el)}(t_0)$ as

$$\boldsymbol{\eta}_{(el)}(t_0) = \left[\boldsymbol{\Phi}_{(el)}^{\mathrm{T}}\mathbf{K}_0\boldsymbol{\Phi}_{(el)}\right]^{-1}\boldsymbol{\Phi}_{(el)}\mathbf{K}_0\mathbf{d}_{(el)}(t_0)\,. \tag{20}$$

For the subsets $\boldsymbol{\Phi}_{(rig)}$ and $\boldsymbol{\Omega}_{(rig)} \equiv \mathbf{0}$ of modes and frequencies related to rigid body displacements,

$$\boldsymbol{\eta}_{(rig)}(t_0) = \boldsymbol{\Phi}_{(rig)}^{\mathrm{T}}\mathbf{M}_1\mathbf{d}_{(rig)}(t_0)\,. \tag{21}$$

The latter expression is given in the books on structural dynamics for all modes (they just write $\mathbf{M}$), but is generically valid only as proposed. Equation (20) is obviously not applicable to (time-varying) rigid body displacements. Several numerical applications in the wider framework of the hybrid boundary element method have attested the consistency of these developments [18, 20, 24].

4 Numerical examples

Barros [25] applied the present developments to assess some 2D and 3D frame and truss structures proposed in the classical structural dynamics books by Weaver and Johnston [16], Paz and Leigh [27] and Petyt [28]. A few 2D examples by Weaver and Johnston [16] are discussed in the following. Some more examples as well as some paramount conceptual issues are discussed presently.

4.1 A three-bar plane truss [16]

The plane truss on the left of Fig. 2 is the example 3.4 by Weaver and Johnston [16] and explored in several parts of their book. We choose this example for its simplicity, which nevertheless enables some important – and hitherto unheard of – conclusions related to structural dynamics. Although the technical literature – and so do Weaver and Johnston [16] – as a rule only requires a bar's cross section area and its length as the geometrical properties for a truss element, our developments show that the cross section moment of inertia is of paramount relevancy. For this sake, we suggest that all bars in this example have hollow circular cross sections with 0.4 *m* of external diameter and thickness of approximately 5.2 *mm*, 3.1 *mm* and 4.15 *mm*, respectively, in such a way that the cross section areas of the bars be exactly 10 in^2, 6 in^2 and 8 in^2, as originally proposed. This is shown in Table 2, which also gives the bar lengths corresponding to 10, 6 and 8 inches. The second last row in Table 2 gives the slenderness ratio of the bars, which are unlikely to undergo relevant buckling effects. The last row displays a slenderness measure proposed by Weaver and Johnston [16] in their chapter on the *component-mode method for trusses* [13]. (An alternative study is carried out by Barros [25] using bars with hollow square cross sections). The material is steel, with elasticity modulus $3\times10^4\, k/in^2$, which is approximately $206.843\, GPa$, to be entirely consistent with Weaver and Johnston's data. The material specific density is $7.35\times10^{-7}\, k\text{-}s^2/in^4$, or, approximately, $7854.87\, kg/m^3$. Although all quantities in the present development are displayed with up to six figures of precision, all unit transformations and all numerical evaluations are actually carried out with 20 digits of precision in the software Maple [26].

Table 1. Geometrical properties for the plane truss of Fig. 2 (adapted from [16])

Tube properties	Bar 1 (nodes 1-2)	Bar 2 (nodes 1-3)	Bar 3 (nodes 2-3)
Diameter (m)	0.4	0.4	0.4
Thickness (m)	$\sim 5.20166\times10^{-3}$	$\sim 3.10451\times10^{-3}$	$\sim 4.15028\times10^{-3}$
Cross section area A (m^2)	6.4516×10^{-3}	3.87096×10^{-3}	5.16128×10^{-3}
Moment of inertia I_z (m^4)	$\sim 1.25720\times10^{-4}$	$\sim 7.62268\times10^{-5}$	$\sim 1.01106\times10^{-4}$
Length L (m)	6.35	3.81	5.08
Slenderness ratio	~ 45.4889	~ 27.1507	~ 36.2956
Ratio AL^2/I_z	~ 2069.24	~ 737.159	~ 1317.37

The left of Fig. 2 is a drawing from a didactical Maple [26] code for general plane frames (Dumont's unpublished lecture notes on matrix structural analysis, 1995), where small (blue) triangles and squares at the nodes represent support displacement and rotation restrictions, whereas (red) circles at the bars' extremities represent eventual hinges. Hinged bars have their hinges specifically considered – to be dealt with according to Section 2.2 – and node rotational degrees of freedom (dof) to which there is no stiffness attached are restricted. The present problem, with three truss elements and three nodes, has only three displacement degrees of freedom: the horizontal displacement at node 1 and both horizontal and vertical displacements at node 2. Since a truss element has no rotational stiffness at the extremities (hinges), the nodal rotational degrees of freedom are all restricted (as given by the small squares). As proposed by Weaver and Johnston [16], the simple plane truss on the left of Fig. 2 is subjected to a point force acting horizontally at node 2 and given as a succession of five linear segments of time, as shown on the right (values originally given in *kip*).

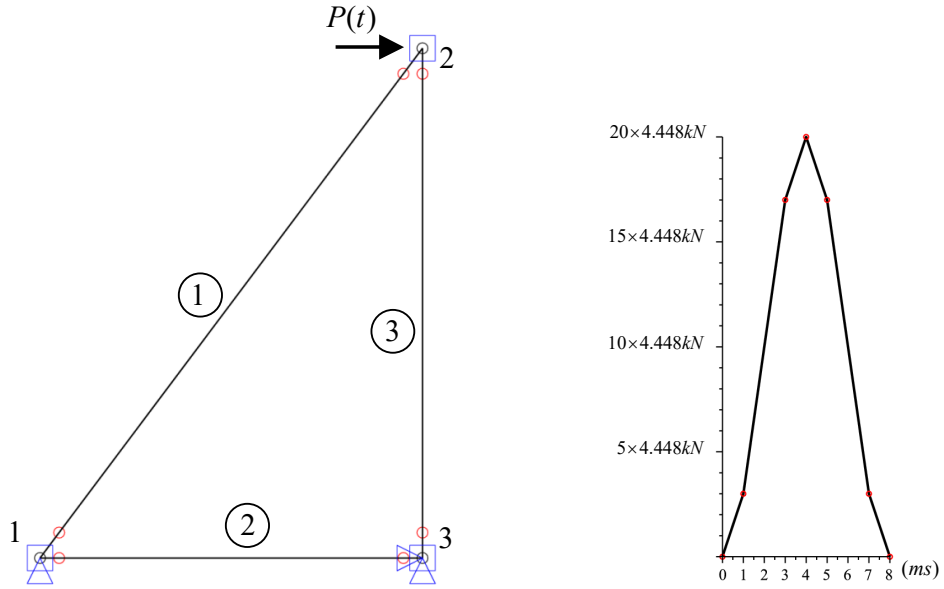

Figure 2. Plane truss (left) submitted to a piecewise-linear force (right) at node 2 [16]

Table 2 shows in the first row the three eigenfrequencies for the truss analyzed as classically, which are also the values given by Weaver and Johnston [16] (with four digits of precision). An analysis of this problem with two and three more terms in the frequency power series of Eq. (11) shows that the series does not converge, which means that the space discretization of this truss with three nodes and three dof is a too coarse one. A second analysis is carried out considering a middle node in each bar [which leads to stiffness matrix cases (1, 0) and (0, 1) of Section 2.2], then with a total of 6 nodes and 12 dof, with results for the eigenfrequencies given in Table 3. A third analysis, with each physical truss element represented as three bars [stiffness matrix cases (1, 0), (0, 0) and (0, 1) of Section 2.2], with a total of 9 nodes and 21 dof, leads to the frequency results of Table 4. We

may conclude from comparing the results of Tables 3 and 4 that the second analysis with 12 dof and three mass matrices quite accurately represents the truss's dynamic behavior when up to the first 6 vibration modes are activated by some applied load. By the way, the completely wrong vibration modes for the truss discretized with three nodes and one mass matrix is given in Fig. 3 [configurations with three mass matrices would be different and still wrong, as the power series of Eq. (11) does not converge]. The vibration modes for the second analysis, with 6 elements, 6 nodes, 12 dof and 3 mass matrices are correct within several digits of precision and are represented in Fig. 4: there is of course no correlation with the vibration modes of the too coarse analysis. The deformed configuration of the truss at the time instant $t = 0.01\ s$ for the piece-wise linear pulse represented on the right of Fig. 2 is given in Fig. 5 for both the coarse and the more adequate meshes and one concludes once more how wrong some numerical results may become if one is not aware of the issues treated in this paper and just follows a text book. The horizontal displacement of the top node of this truss for the applied load is given as a function of time in Fig. 6 for both the coarse and the adequate mesh discretizations. This coarse mesh result (with one mass matrix) is also displayed by Weaver and Johnston [16], but they are probably inadvertently referring to some applied damping, as their data slightly differ from the dash line results of Fig. 6.

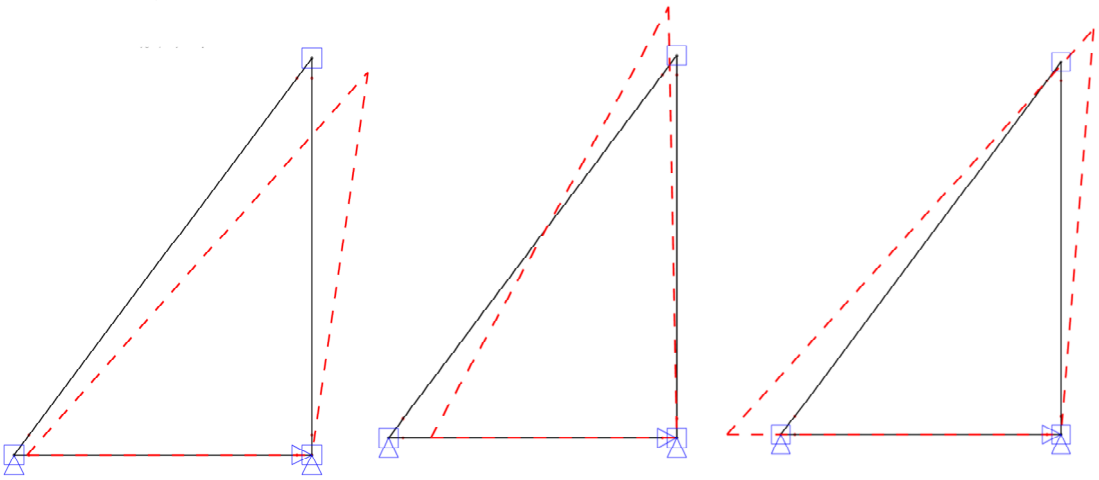

Figure 3. Vibration modes 1, 2 and 3 of the plane truss of Fig. 2 discretized with 3 elements, 3 nodes, 3 dof and one mass matrix (eigenfrequencies given in Table 2)

Table 2. Eigenfrequencies (*rad/s*) for the plane truss of Fig. 2 with 3 nodes and 3 dof

Frequency number	1 mass matrix	2 mass matrices	3 mass matrices
1	419.951	282.412	235.100
2	1167.71	897.417	609.013
3	1861.80	1055.98	945.186

Table 3. Eigenfrequencies (*rad/s*) for the plane truss of Fig. 2 with 6 nodes and 12 dof

Frequency number	1 mass matrix	2 mass matrices	3 mass matrices
1	170.147	169.001	168.975
2	265.100	263.314	263.273
3	493.146	489.690	489.606
4	646.512	606.835	597.730
5	882.701	792.752	774.154
6	1272.42	1173.75	1146.07
⋮	⋮	⋮	⋮
10	3585.07	3234.81	3150.03
11	4965.06	4401.01	4237.59
12	5989.27	5141.13	4804.40

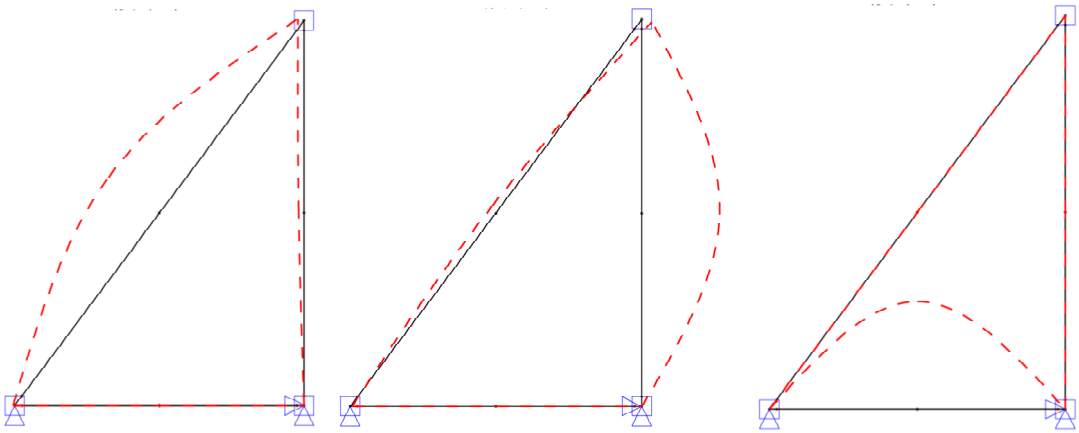

Figure 4. Vibration modes 1, 2 and 3 of the plane truss of Fig. 2 discretized with 6 elements, 6 nodes, 12 dof and 3 mass matrices (eigenfrequencies given in Table 3)

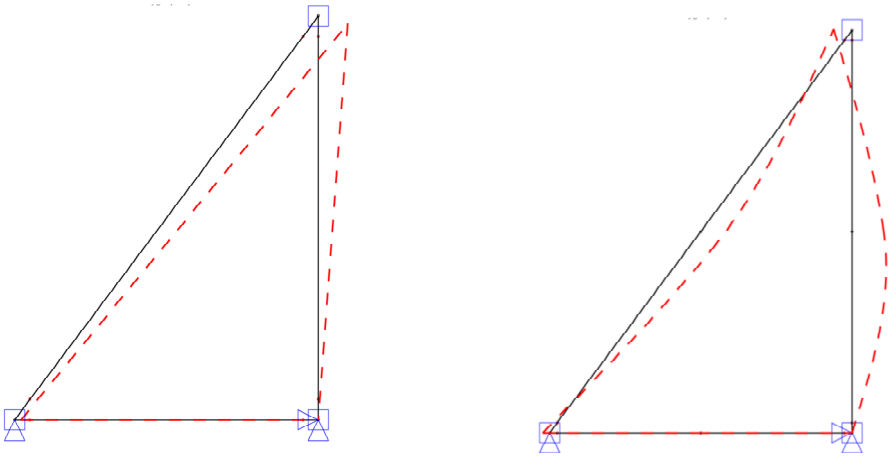

Figure 5. Deformed configuration at the time instant $t = 0.01$ seconds of the example of Fig. 2 for the indicated pulse, with the truss discretized with 3 elements, 3 nodes, 3 dof and one mass matrix (left) as well as 6 elements, 6 nodes, 12 dof and 3 mass matrices

Table 4. Eigenfrequencies for the plane truss of Fig. 2 with 9 nodes and 21 dof

Frequency number	1 mass matrix	2 mass matrices	3 mass matrices
1	169.142	168.975	168.975
2	263.535	263.273	263.272
3	490.108	489.606	489.604
4	603.248	594.778	594.353
5	774.992	764.290	763.566
6	1146.56	1129.24	1128.01
⋮	⋮	⋮	⋮
10	2212.97	2130.13	2119.03
11	3021.91	2670.59	2592.64
12	3640.72	3392.39	3332.55

It should be mentioned that Weaver and Johnston [16] were most probably aware of the bad results they displayed for the coarse mesh of Fig. 2, as they present a similar simple truss study in their section on *component-mode method for trusses* (example 10.4) and propose a dramatic improvement by explicitly considering flexural modes (a conceptually restricted development, actually). This example, which has basically the same geometry of the truss of Fig. 2 (just horizontally reversed) with

node 1 completely restricted to displacements, was also assessed in the frame of the present advanced modal analysis. In this example, the vertical and inclined bars have the same properties and I_z is proposed such that the ratio $AL^2/I_z = 250$, which corresponds to a quite unrealistic cross section, although Weaver and Johnston asserts exactly the contrary. The first three vibration modes given by Weaver and Johnston [16] are visually corroborated by us, but the fourth mode differs significantly. The first six eigenfrequencies given by them compare well with our more accurate analysis (with bars subdivided), as reproduced in Table 5, which is certainly due to the extremely high moment of inertia they propose: just compare with the results obtained with the data of Table 1.

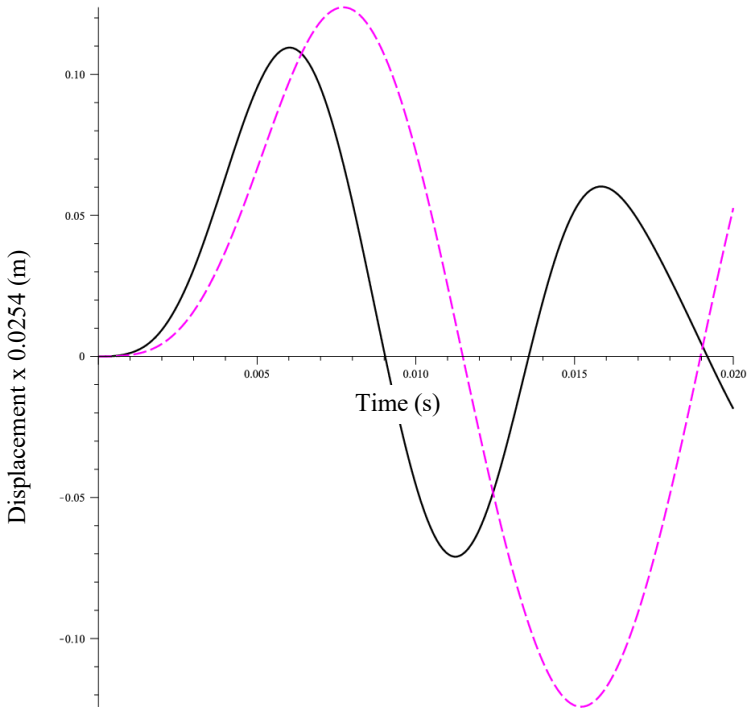

Figure 6. Horizontal displacement of the top node of the plane truss of Fig. 2 for discretizations with 3 bars, 3 nodes, 3 dof and one mass matrix (dash line) as well as 6 elements, 6 nodes, 12 dof and 3 mass matrices (solid line)

Table 5. Eigenfrequencies (*rad/s*) for the plane truss of Fig. 10.14 of Weaver and Johnston [16], which is similar to the structure on the left of Fig. 2 with node 1 also horizontally restricted

Frequency number	1 mass matrix	4 mass matrices	Weaver and John
1	0.204021	0.203962	0.203
2	0.316677	0.316586	0.317
3	0.800003	0.795624	0.796
4	1.19562	1.18870	1.189
5	1.70362	1.66331	1.668
6	2.18658	2.14458	2.171
7	2.92301	2.88231	3.034
8	3.16742	3.03699	3.163
9	4.03510	3.56016	3.628
10	5.98138	5.20551	5.146
11	6.56036	5.52458	5.575
12	7.37174	6.77306	8.267

By the way, the same example of Fig. 2 is investigated once more for the moments of inertia given in Table 1 multiplied by 100 (which also corresponds to a quite unrealistic cross section). The results are shown in Tables 7 and 8, which are to be directly compared with the original results of Tables 2 and 3: the transversal inertia effects are always of concern no matter how stiff a physical truss structural bar may be conceived.

Table 7. Eigenfrequencies (*rad/s*) for the plane truss of Fig. 2 with 3 nodes and 3 dof for the moment of inertia of Table 1 multiplied by 100 (to be compared with results of Table 2)

Frequency number	1 mass matrix	2 mass matrices	3 mass matrices
1	419.951	414.080	413.816
2	1167.71	1114.38	1107.13
3	1861.80	1690.36	1639.71

Table 8. Eigenfrequencies (*rad/s*) for the plane truss of Fig. 2 with 6 nodes and 12 dof for the moments of inertia of Table 1 multiplied by 100 (to be compared with results of Table 3)

Frequency number	1 mass matrix	2 mass matrices	3 mass matrices
1	414.092	413.802	413.802
2	1121.06	1106.19	1105.62
3	1594.06	1576.11	1575.12
4	2612.05	2513.47	2499.95
5	3078.19	2949.71	2927.71
6	4058.08	3890.98	3863.12
⋮	⋮	⋮	⋮
10	10863.4	9006.23	8352.15
11	15403.8	12707.3	11821.7
12	24902.6	20919.9	20034.4

4.2 A four-panel plane truss presented by Weaver and Johnston [16]

The following numerical study concerns the symmetric plane truss example 3.5 of Weaver and Johnston [16], with eight panels of triangle trusses with a total of 18 nodes. Owing to its symmetry, only half of the truss is discretized with 10 nodes and support conditions at the right extremity entered to simulate either a symmetric or an antisymmetric behavior. The example is shown in Fig. 7 for the case of symmetry. The material is aluminum, with elasticity modulus $69\,GPa$ and material specific density $2620\,kg/m^3$. Weaver and Johnston [16] give as geometrical properties only bar lengths and cross section areas. In order to estimate the bars' moments of inertia, Barros [25] considered 0.4 *m* of external diameter of circular cross sections, but we are redoing the calculations with more slender bars, of just 0.2 *m* of external diameter. The geometrical properties of the bars are shown in Table 9. The second last row in this Table gives the slenderness ratios of the bars, which are unlikely to undergo relevant buckling effects. Observe that bar 12 – on the symmetry axis of the structure – contributes with half of the values of cross section area and moment of inertia in the discretization. Actually, the cross section area of this bar contributes only in the symmetric part of the simulation, whereas the moment of inertia contributes only in an antisymmetric simulation that uses more than one mass matrix. The numerical model has a total of 12 truss elements, 10 nodes and 14 dof.

The vertical translation of node 6 in Fig. 7 is graphically given by Weaver and Johnston [16] and could be visually checked by Barros [25] for one mass matrix as closely as possible. However, this is a very coarse implementation, and there is no convergence when more mass matrices are introduced, as shown for the first three eigenfrequencies displayed in Table 10, which actually invalidates all results. We run a second simulation with double the number of bars [stiffness matrix cases (1, 0) and (0, 1) of Section 2.2], with a total of 32 bars, 26 nodes and 60 dof. The corresponding results for the first six modes are given in Table 11 for implementations with one through four mass matrices: convergence can be attained and numerical results are validated for just one mass matrix. Mode shapes, single node responses and whole structure configurations with time (a Maple [26] command enables time

animation) could be most reliably run for any time-dependent force application and are to be displayed in a more extensive version of this paper. The improvements obtained with this example are then of the same quality as for the first example.

Table 9. Geometrical properties for the plane truss example of Fig. 6 (Weaver and Johnston [16])

Tube properties	Bars 1-11	Bar 12	Bars 13-16
Diameter (m)	0.2	-	0.2
Thickness (m)	$\sim 1.00548\times10^{-2}$	-	$\sim 1.55298\times10^{-2}$
Cross section area (m^2)	6×10^{-3}	$6\times10^{-3}/2$	9×10^{-3}
Moment of inertia (m^4)	$\sim 2.71352\times10^{-5}$	$\sim 2.71352\times10^{-5}/2$	$\sim 3.85542\times10^{-5}$
Length (m)	5	5	~ 7.07107
Slenderness ratio	~ 74.3497	~ 74.3497	~ 76.3933
Ratio AL^2/I_z	~ 5527.87	~ 5527.87	~ 11671.9

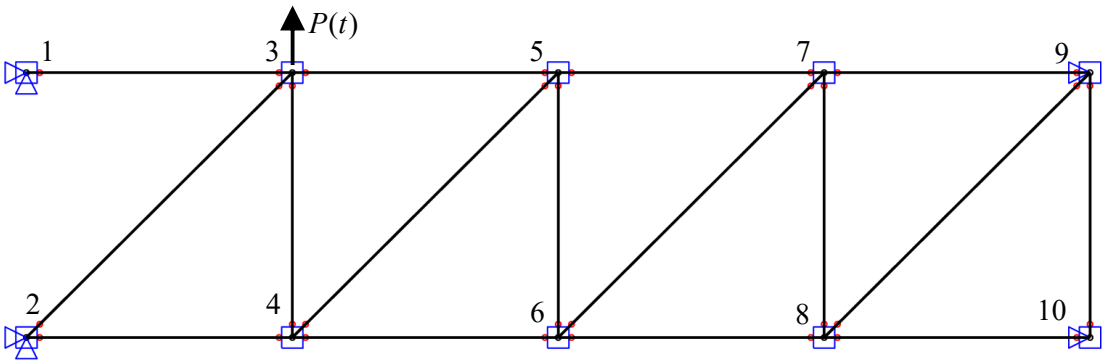

Figure 7. Plane truss submitted to a step force at node 3 (example 3.5 of Weaver and Johnston [16])

Table 10. First eigenfrequencies for the plane truss of Fig. 6 with 16 bars, 10 nodes and 14 dof

Frequency number	1 mass matrix	2 mass matrices	3 mass matrices
1	79.5502	70.6044	66.6298
2	276.627	172.044	128.882
3	520.502	262.323	169.842

Table 11. First eigenfrequencies for the plane truss of Fig. 6 with 32 bars, 26 nodes and 60 dof

Frequency number	1 mass matrix	2 mass matrices	3 mass matrices	4 mass matrices
1	60.0043	59.6827	59.6764	59.6763
2	66.4225	65.9594	65.9483	65.9480
3	66.6907	66.2239	66.2126	66.2123
4	66.7414	66.2739	66.2626	66.2623
5	87.5428	87.2359	87.2292	87.2290
6	132.679	131.781	131.761	131.760

The attempt to improve results in terms of the *component-mode method for trusses* [13] has motivated Weaver and Johnston [15] to run a series of simulations for a plane truss similar to the one of Fig. 7, obtained by letting the nodes at the right extremity to completely displace and reversing the figure horizontally. Weaver and Johnston's thesis is that, when such a truss has a sufficiently large number of panels, the results obtained in a classical implementation should coincide – for practical applications – with results obtained in a more sophisticated approach, such as proposed by Hurty [13].

We checked that with our more precise numerical tool and can only partially agree with the thesis. To start with, we run the four-panel truss of Fig. 7 again, for nodes 9 and 10 free to displace and with the same properties given in Table 9, with either 10 or 26 nodes, as before.

The main difference is that, with the nodes on the right extremity free to displace in Fig. 7, the horizontal bars are no longer submitted to total elongation restraint and the structure tends to behave like a cantilever beam (small displacements considered all along the analyses). Instead of showing the structure's eigenfrequencies in tables, as before, we attempt to diagnose the whole problem graphically, as shown in Fig. 8, for an analysis with 16 bars, 10 nodes and 16 dof compared with the analysis with 32 bars, 26 nodes and 64 dof using one through four mass matrices (solid, long dash, dash dot and dash lines, respectively). The results are still bad for the 10 nodes analysis, although not as bad as in the original example of Fig. 7. The first eigenfrequency seems to not differ much, this time (compare with the original results in Tables 10 and 11), but the values for 10 nodes in Fig. 8 actually converge from 57.6116 to 51.2334 *rad/s*, while the correct value obtained for 26 nodes is 50.48300 *rad/s* (7 digits accuracy).

This cantilever beam behavior is in fact the effect explored by Weaver and Johnston [15] in their example 10.5. They use the geometry of Fig. 7 for one extremity completely free to displace, but assuming that all truss members have the same properties ρ, E, A and I_z, such that $AL^2/I_z = 2250$, for L the panel dimension, in a study for one through six panels and a step force vertically applied at the top middle of the panel at the free extremity. The bars' cross sections are then bulkier than the ones assumed in the previous example, as shown in the last row of Table 9. The conclusion by Weaver and Johnston [15] is that reasonable responses with one bar as one truss element are obtained for a structure with four or more panels. We run the same cases as described for Fig. 8, this time with the geometry and the mechanical properties given above. A diagnosis in terms of frequency values may be drawn from Fig. 9. In fact, when just a few, low vibration modes are activated by the applied forces, the results may not be so bad. However, they cannot be considered as reliable, particularly because they apply to the very particular case of using a plane truss to simulate a cantilever beam's behavior.

4.3 A complex plane truss

The simply supported complex plane truss on the left of Fig. 10 has a large number of panels, to show that the local behavior of a truss bar may very much influence a structure's global behavior. The dimensions are 9 *m* in the horizontal direction and 16 *m* in the vertical, with nodal coordinates of the 12 nodes multiples of 3 horizontally and of 4 vertically. The material is steel, as in the first example, with $A = 0.006\,m^2$ for all bars and moment of inertia such that $AL^2/I_z = 2500$ for the nominal bar length $L = 5\,m$ as for the diagonal members. This corresponds to a hollow circular cross section with $\sim 0.28952m$ of external diameter and $\sim 6.75430mm$ thickness. (This example was also analyzed with a relation $AL^2/I_z = 250$, which would correspond to a tube with $\sim 0.89660m$ of diameter and $\sim 2.13529mm$ thickness, leading to very stiff truss elements and to results with no flexural contribution at all, but corresponding to an unrealistic structure.)

The structure is first analyzed as shown on the left of Fig. 10, with 12 nodes, 24 bars and a total of 21 dof. A second analysis is carried out with double the number of bars, corresponding to 36 nodes and a total of 93 dof. The eigenfrequencies for both sets of analysis are shown in Fig. 11 for one through four mass matrices (solid, long dash, dash dot and dash lines, respectively). No numerical convergence is achieved in the analyses using 24 bars and no result coming from such a discretization should be considered reliable. On the other hand, the results with 48 bars look excellent and convergence is attained as the number of mass matrices increases. A direct comparison of eigenmodes for the structure with 24 and 48 bars is not a simple task. The first three eigenmodes of the plane truss with 24 and 48 bars are shown in Figs. 12 (one mass matrix) and 13. In the reliable discretization with 48 bars it is not possible to single out the bars' flexural contribution in the modal configurations. The deformed, now reliable, configuration for a step force applied horizontally on the top left node is shown on the right of Fig. 10 for the time instant $t = 0.1\ s$. The horizontal displacement of the top left node, as related to the static effect of the load (an amplification factor of almost 2 is observed), is given in Fig. 14 for up to *0.2 s*. The result with 48 bars and 93 dof is the solid (black) line, which is basically the same graphic for any number of mass matrices. The corresponding result for 24 bars and one mass matrix is given in dash (red) line, whereas the result for four mass matrices (always for just 21 dof) is in longdash (blue) line. As we see, any results with 24 bars are just wrong.

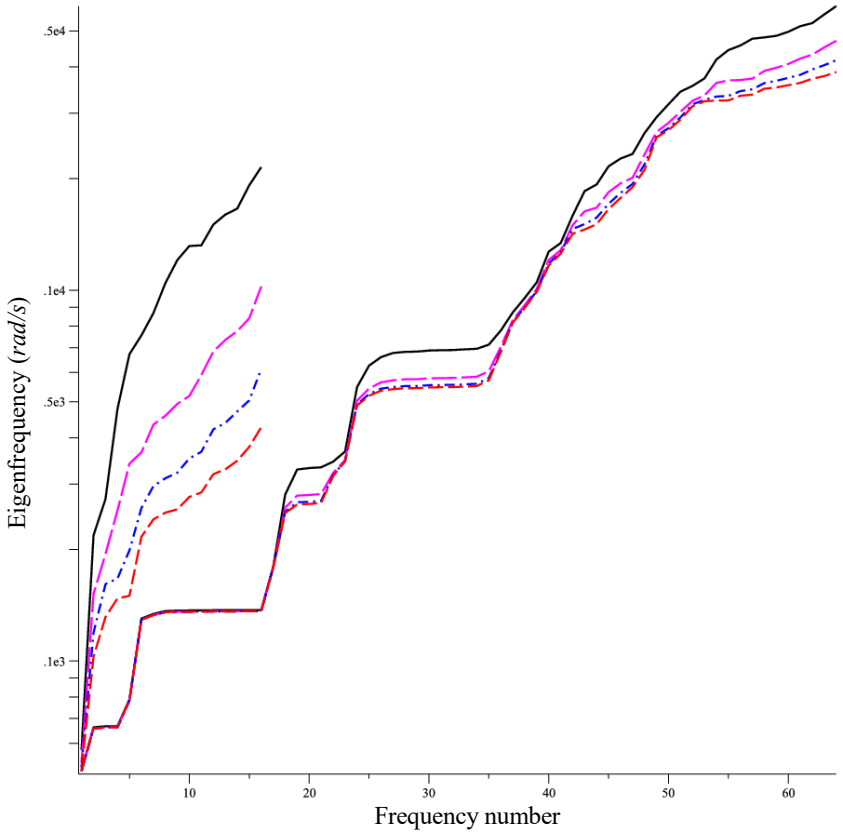

Figure 8. Eigenfrequencies for the plane truss of Fig. 7 with nodes on the right free to displace

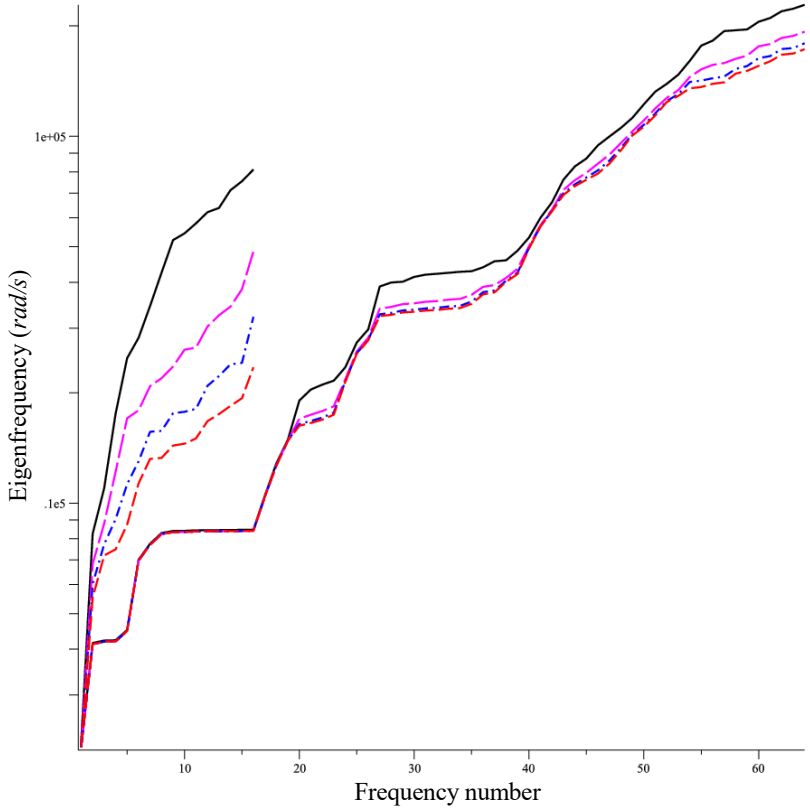

Figure 9. Eigenfrequencies as in Fig. 8 for a plane truss with stiffer bars

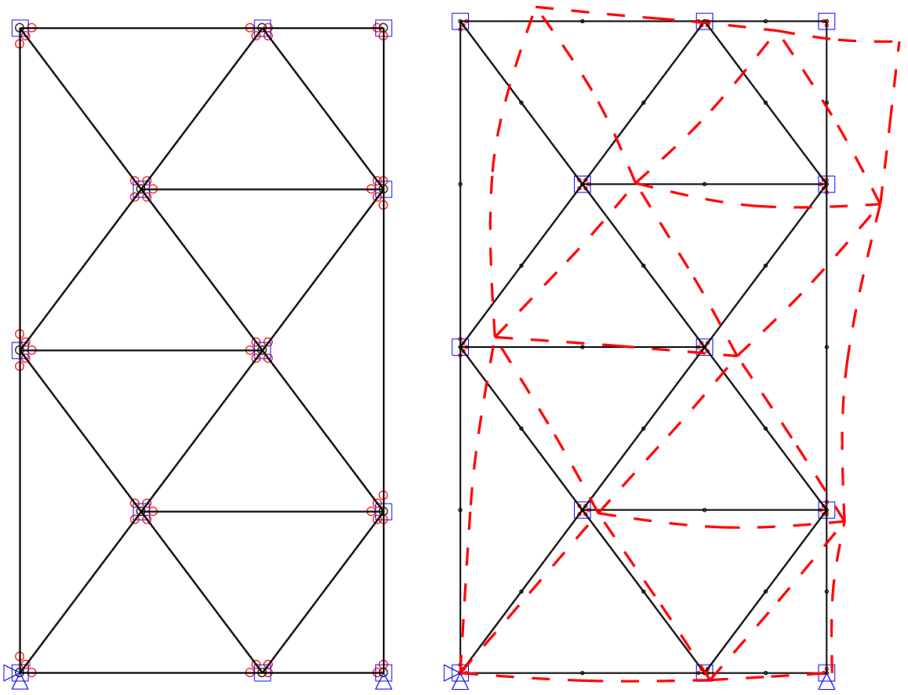

Figure 10. Complex truss of Section 4.3 and displacement configuration for t = 0.1 *s*

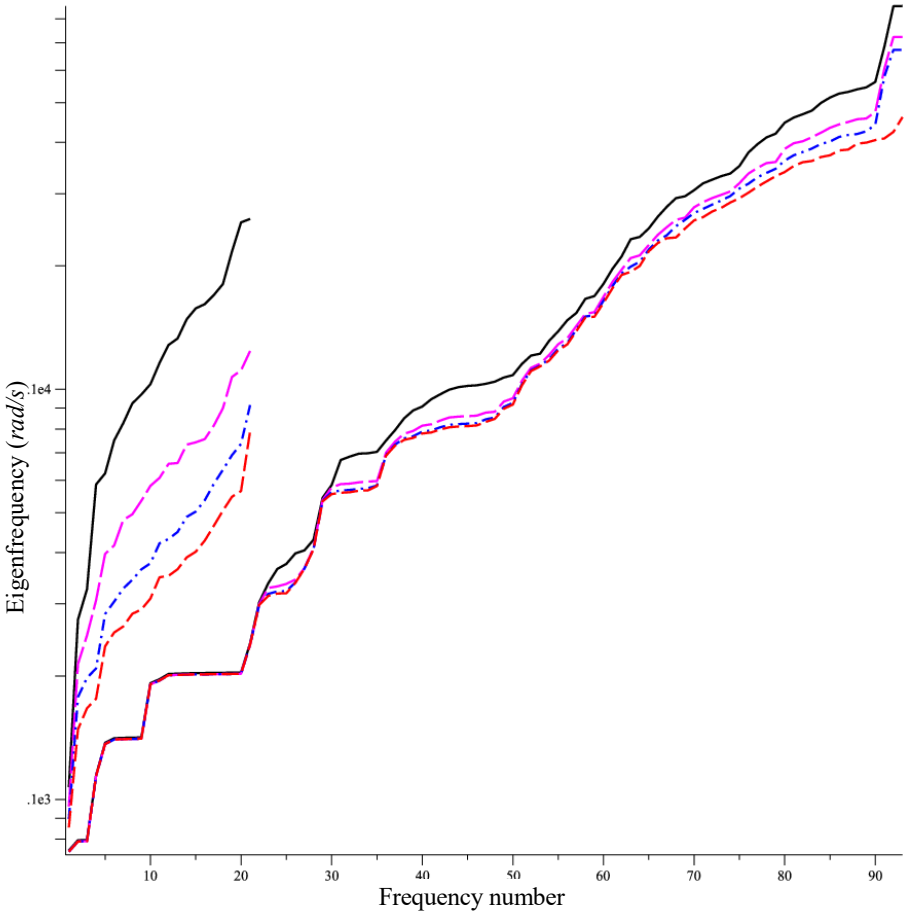

Figure 11. Eigenfrequencies of the plane truss of Fig. 10 for discretizations with 24 and 48 bars

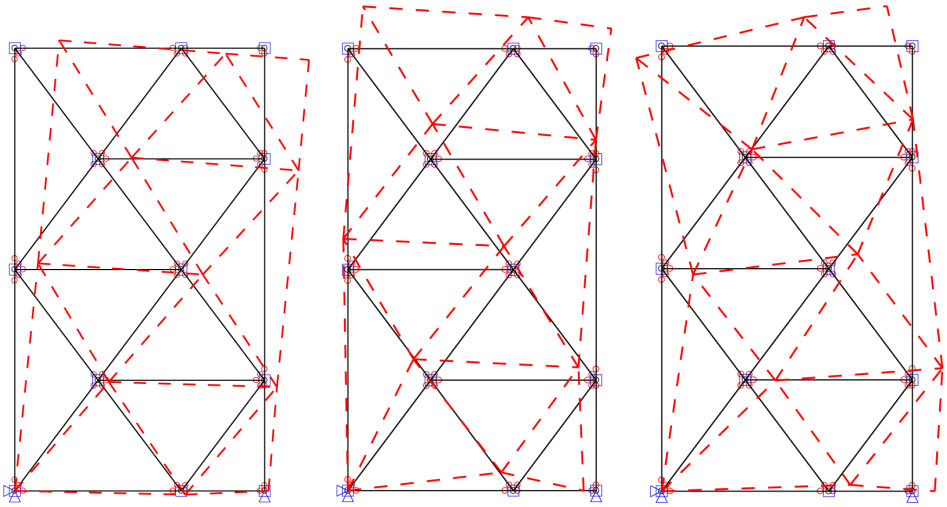

Figure 12. Vibration modes 1, 2 and 3 of the plane truss of Fig. 10 discretized with 24 bars

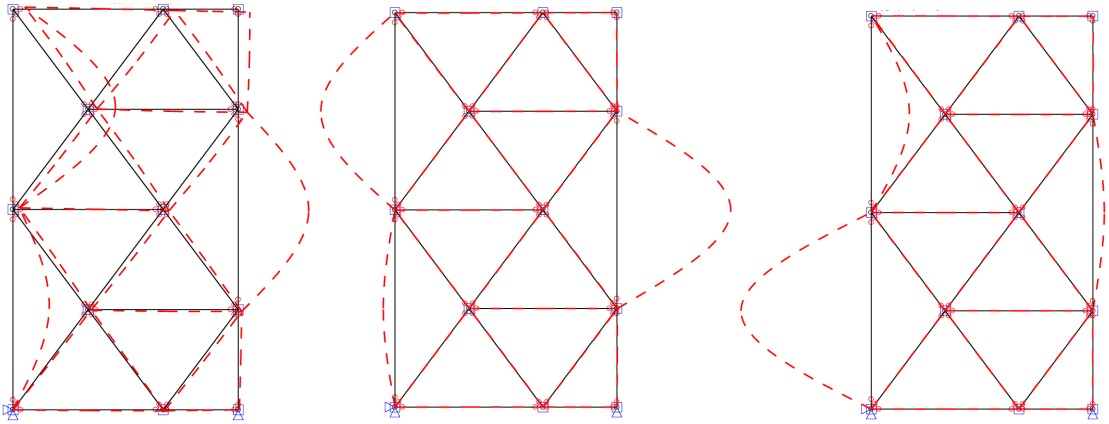

Figure 13. Vibration modes 1, 2 and 3 of the plane truss of Fig. 10 discretized with 48 bars

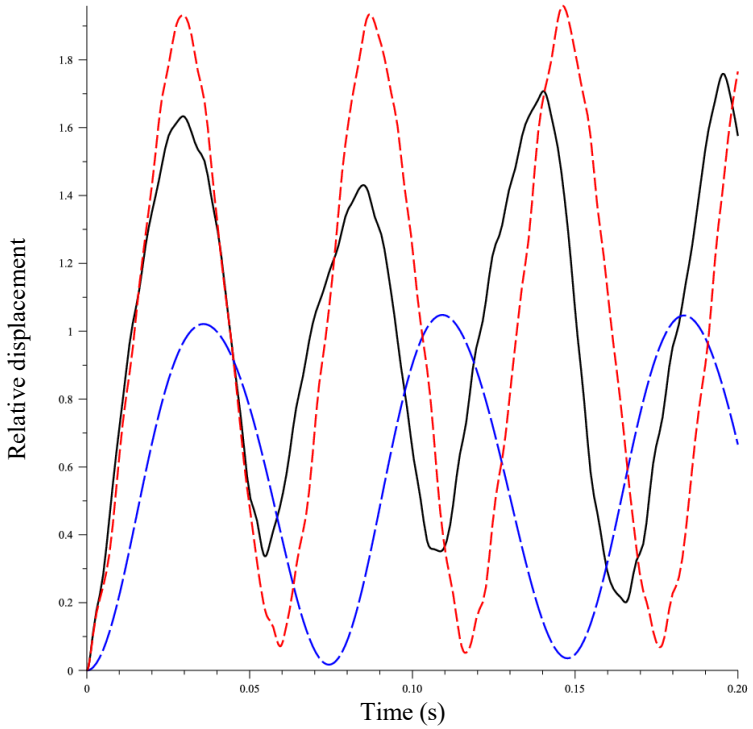

Figure 14. Horizontal displacement of the top left node of the plane truss of Fig. 10 for 24 bars and one (dash line) or four mass matrices (long dash line) as well as with 48 bars (solid line)

5 Concluding remarks

Barros [25] analyzed the plane frame model proposed as example 6.13 by Weaver and Johnston [16], which had already been the subject of analysis by Prazeres [21]. A three-dimensional frame model proposed by Petyt [28] was investigated by Barros [25] as well as by Carvalho [29]. The analyses by Barros [25], Prazeres [21] and Carvalho [29] – which had research interests independent from each other – had in common the application of the generalized modal analysis proposed by Dumont and co-workers. The results obtained in [21, 25, 29] corroborate that the models proposed by Weaver and Johnston [16] and also by Petyt [28] are adequate if not too high vibration modes are activated. On the other hand, another 3D frame model proposed by Paz and Leigh [27] was found out completely inadequate by Barros [25]. One may conclude that, since a beam structural model inherently takes into account the moment of inertia, the classical structural dynamics developments for 2D or 3D frames are usually of good quality – if not too high vibration modes are activated.

On the other hand, as carried out by Barros [25] in his own investigations of the plane trusses of Figs. 2 and 7 corresponding to examples 3.4 and 3.5 by Weaver and Johnston [16], as well as for a three-dimensional truss model proposed by Paz and Leigh [27], the classical understanding of a hinged bar under dynamic loading must be completely revised. The attempts in References [11-16] are just – in part misled – approximations of the correct structural and linear algebra treatment proposed by Dumont and co-workers in a wide framework, as referenced here.

The main conclusion to be drawn from the developments of the generalized modal analysis for boundary and finite elements – and shown to be extensive to frame structures – is that the classical approach of a stiffness matrix plus a mass matrix (and eventually a matrix for viscous damping) is just a truncation. In structural dynamics there should not be such a thing as a truss element. Moreover, it should be a surprise that, if for a structure made of slender beam elements (local and global buckling duly prevented), the global effect of axial deformation may be neglected in the presence of the flexural effect, why is that that we feel justified to neglect the effect of flexural deformations in a truss element? This paradox is solved here.

Analyses using lumped matrices, for instance, may work for large numbers of degrees of

freedom, or because we know or hope that low vibration modes dominate and there are so many more uncertainties to be taken into account (liability of a structure to buckling, non-linear effects, stiffening and damping of the joints). It should never be taken for granted in a frame structure – particularly if there are hinges – that a numerically modeled node should occur only where there are physical joints.

The use of the proposed generalized modal analysis is not compulsory in structural dynamics and sometimes just shows that a proposed geometric mesh discretization is too coarse, as seen in Fig. 11 for the example of Fig. 10. A convergence analysis is always advised – most importantly in the text books. The computationally simplest and conceptually most enriching refinement should be in the frequency domain: just allow for a second mass matrix in your model – one term more in the power series – and compare results. An executable Fortran module for the solution of both real and complex-symmetric, associate non-linear eigenvalue problem may be requested directly to the first author [10]. The module can be easily accessed from inside a Fortran, C, Matlab or Maple code.

It should be once more remarked that the longitudinal and transversal displacement shapes for a beam element – whether or not hinged – come out to be the ones of the static analysis added by higher order polynomials that behave as bubble functions: this is obtained by just developing the displacements of Eqs. (1) and (3) as frequency power series.

Acknowledgements

This research work was supported by the Brazilian agencies CAPES, CNPq and FAPERJ.

The first author is thankful to his colleague Raul Rosas e Silva for the vivid technical discussions on some of this paper's subjects held along the years.

References

[1] C. A. Aguilar. *Comparação do desempenho computacional da técnica de superposição modal avançada com a técnica da transformada de Laplace*, M. Sc. Thesis, PUC-Rio, Brazil, 2008.

[2] N. A. Dumont and C. A. Aguilar. Linear algebra issues in a family of advanced hybrid finite elements, *in J. Murín, V. Kutis and R. Duris, eds, CMAS2009 - International Conference on Computational Modelling and Advanced Simulations*, 15 pp. on CD, Bratislava, Slovak Republic, 2009.

[3] H. Dubner and J. Abate. Numerical inversion of Laplace transforms by relating them to the finite Fourier cosine transform, *Journal of the Association for Computing Machinery*, vol. 15, n. 1, pp. 115-123, 1968.

[4] K. S. Crump. Numerical inversion of Laplace transforms using a Fourier series approximation, *Journal of the Association for Computing Machinery*, vol. 23, pp. 89-96, 1976.

[5] F. R. De Hoog, J. H. Knight and A. N. Stokes. An improved method for numerical inversion of Laplace transforms, *SIAM Journal on Scientific and Statistical Computing*, 3, 357-366, 1982.

[6] T. H. H. Pian. Derivation of element stiffness matrices by assumed stress distribution, *AIAA Journal*, Vol. 2, pp 1333-1336, 1964.

[7] J. S. Przemieniecki. *Theory of Matrix Structural Analysis*, McGraw-Hill Book Company: New York, 1968.

[8] N. A. Dumont and R. Oliveira. From frequency-dependent mass and stiffness matrices to the dynamic response of elastic systems, *International Journal of Solids and Structures*, vol. 38, n. 10-13, pp. 1813-1830, 2001.

[9] N. A. Dumont. On the Inverse of Generalized Lambda Matrices with Singular Leading Term, *International Journal for Numerical Methods in Engineering*, vol 66, n. 4, pp. 571-603, 2006.

[10] N. A. Dumont. On the solution of generalized non-linear complex-symmetric eigenvalue problems, *International Journal for Numerical Methods in Engineering*, Vol. 71, pp 1534-1568, 2007.

[11] H. Voss. A new justification of finite dynamic element methods, *International Series of Numerical Mathematics,* vol. 83, pp. 232-242, 1987.

[12] F. Triebsch. *Eigenwertalgorithmen für symmetrische lambda-Matrizen*. Ph.D. Thesis, Technische Universität Chemnitz-Zwickau, Germany, 1995.

[13] W. C. Hurty. Dynamic analysis of structural systems using component modes, *AIAA J.*, vol.3, n. 4, pp. 678-685, 1965.
[14] R. R. Craig Jr and M. C. C. Bampton. Coupling of substructures for dynamic analysis, *AIAA J.*, vol. 6 n. 7, pp. 1313-1319, 1968.
[15] W. Weaver Jr. and C. L. Loh. Dynamics of trusses by component-mode method, *ASCE J. Struct. Eng.*, vol 111, n. 12, pp 2526-2575, 1985.
[16] W. Weaver Jr. and P. R Johnston. *Structural Dynamics by Finite Elements*, New Jersey, 1987.
[17] N. A. Dumont and R. A. P. Chaves. General time-dependent analysis with the frequency-domain hybrid boundary element method, *Computer Assisted Mechanics and Engineering Sciences*, vol. 10, pp. 431-452, 2003.
[18] R. A. P. Chaves. *O Método Híbrido Simplificado dos Elementos de Contorno Aplicado a Problemas Dependentes do Tempo*, Ph. D. Thesis, PUC-Rio, Brazil, 2003.
[19] N. A. Dumont and P. G. C. Prazeres. A family of advanced hybrid finite elements for the general analysis of time-dependent problems and non-homogeneous materials, *XXV CILAMCE – XXV Iberian Latin-American Congress on Computational Methods in Engineering*, Recife, 15 pp. on CD, 2004.
[20] N. A. Dumont. An advanced mode superposition technique for the general analysis of time-dependent problems, *Advances in Boundary Element Techniques VI*, eds. Selvadurai APS, Tan CL, Aliabadi MH; CL Ltd.: England, pp. 333-344, 2005.
[21] P. G. C. Prazeres. *Desenvolvimento de Elementos Finitos Híbridos para a Análise de Problemas Dinâmicos com o Uso de Técnicas Avançadas de Superposição Modal*, M. Sc. Thesis, PUC-Rio, Brazil, 2005.
[22] A. C. Oliveira. *Um Modelo de Interação Dinâmica entre os Elementos de uma Via Férrea*, M. Sc. Thesis, PUC-Rio, Brazil, 2006.
[23] N. A. Dumont and A. C. Oliveira, A Dynamic interaction model of railway track structural elements, *XXVII CILAMCE – XXVII Iberian Latin-American Congress on Comp. Methods in Engineering*, Belém, 16 pp. on CD, 2006.
[24] N. A. Dumont. Advanced Mode-Superposition Analysis with Hybrid Finite Elements, *XIII DINAME - The International Symposium on Dynamic Problems of Mechanics*, Angra dos Reis, Brasil, 10 pp. on CD, 2009.
[25] R. N. Barros. *Análise dinâmica de treliças e pórticos tridimensionais usando uma técnica avançada de superposição modal*, M. Sc. Thesis, PUC-Rio, Brazil, 2017.
[26] Maple 15. *Maplesoft, a division of Waterloo Maple Inc*., Waterloo, Ontario.
[27] M. Paz and W. Leigh. *Structural Dynamics: Theory and Computation*, Springer Series, 2004.
[28] M. Petyt. *Introduction to Finite Element Vibration Analysis*, Cambridge, 2010.
[29] W. T. Carvalho. *Tratamento de algumas questões conceituais e numéricas na análise de problemas de autovalores generalizados não lineares no método híbrido simplificado dos elementos de contorno*, Ph. D. Thesis, PUC-Rio, Brazil, 2017.